Raman heterodyne interference: Observations and analytic theory

M. Mitsunaga, E. S. Kintzer, and R. G. Brewer
IBM Research Laboratory, San Jose, California 95193
and Department of Applied Physics, Stanford University, Stanford, California 94305
(Received 21 December 1984)

The recently developed technique of Raman heterodyne detection has unveiled a new interference effect in the Zeeman spectrum of hyperfine transitions of impurity-ion solids. An earlier theory had been developed to explain the basic Raman heterodyne process which involves the resonant interaction of a three-level quantum system with coherent optical-frequency and radiofrequency fields. However, it was not realized that impurity-ion crystals can generate more than one type of Raman heterodyne signal and that these signals can interfere. This article describes two examples of interference where one originates from two or more inequivalent nuclear sites and the other from a single site that exhibits interference among Zeeman transitions. An analytical theory covering these two cases is presented and compared to observations for the impurity-ion crystals Pr^{3+}:$YAlO_3$ and Pr^{3+}:LaF_3, the interference behavior in the two being dramatically different.

I. INTRODUCTION

This article describes an unexpected interference phenomenon[1] that was discovered recently in an impurity-ion crystal using an optical heterodyne technique[2–4] based on the coherent Raman effect. To review, Raman heterodyne detection involves the simultaneous excitation of a three-level quantum system by two coherent fields as in Fig. 1, an optical field of frequency Ω that resonantly excites an electron transition $2\rightarrow 3$ and a radiofrequency field of frequency ω that excites a nuclear magnetic resonance transition $1\rightarrow 2$. The resonant Raman process generates an optical field at the sum frequency $\Omega'=\Omega+\omega$ and with the driving field Ω, a heterodyne beat signal results at the difference frequency $\omega=|\Omega'-\Omega|$. In this way, nuclear magnetic resonances, either spin-coherent transients or continuous-wave signals, can be monitored with great sensitivity.

A perturbative calculation[2,3] shows that the Raman heterodyne signal

$$S\sim\mu_{12}\mu_{23}\mu_{31} \tag{1.1}$$

depends on the triple product of the three matrix elements connecting these states. Since each matrix element is phase dependent and appears linearly, interference can occur. An example is given in Fig. 2 for the impurity ion $Pr^{3+}(I=\frac{5}{2})$ in the host crystal $YAlO_3$ where the electron-hyperfine energy-level diagram of Fig. 1 applies. Here, the interference arises from two inequivalent nuclear sites that generate signals $S_{1,2}$ of opposite sign. For other experimental conditions, interference can also occur in a single nuclear site among Zeeman-split hyperfine transitions. In contrast, most other spectroscopic techniques yield signals which are a function of the square of the relevant transition matrix elements and therefore are immune to these interferences.

In this article, we extend our earlier study[1] by develop-

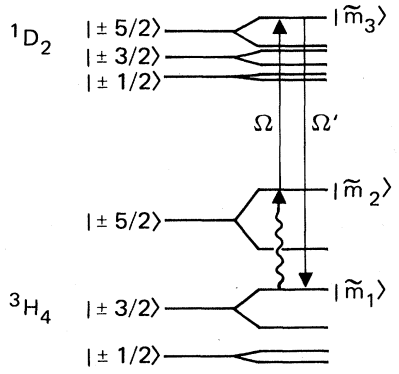

FIG. 1. Zeeman-split hyperfine energy diagram for the Pr^{3+} $^3H_4\rightarrow{}^1D_2$ transition, the lowest crystal-field components of Pr^{3+}:$YAlO_3$ or Pr^{3+}:LaF_3 showing the coherent Raman process (not to scale) for Zeeman-split states $|\tilde{m}_1\rangle$, $|\tilde{m}_2\rangle$, and $|\tilde{m}_3\rangle$.

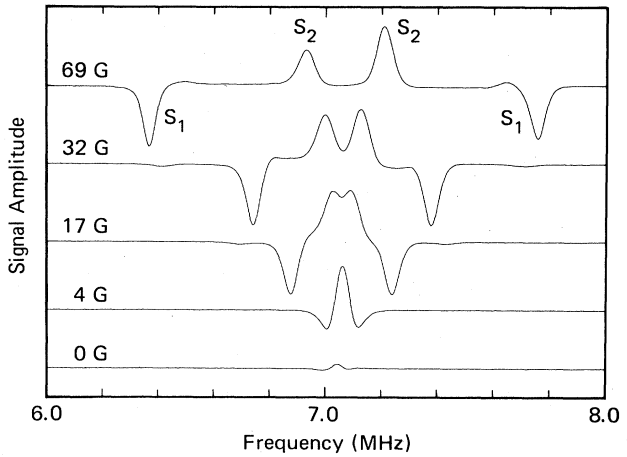

FIG. 2. Observed Raman heterodyne beat spectrum in absorption for the $^3H_4|\pm\frac{3}{2}\rangle\leftrightarrow|\pm\frac{1}{2}\rangle$ transitions of 0.1 at. % Pr^{3+}:$YAlO_3$ as a function of $H_0(\chi=33.6°)$ where $\mathbf{H}_{rf}||c$ axis and the sign reversal in S_1, S_2 for the two sites is evident. Interference is complete at $H_0=0$.

ing a detailed analytic theory and by presenting observations of site and Zeeman interferences in the impurity-ion crystals Pr^{3+}:$YAlO_3$ and Pr^{3+}:LaF_3, examples which display quite different behavior. In the accompanying paper,[5] Raman heterodyne site interference is examined by a symmetry analysis using group theory. The two approaches are complementary since the symmetry arguments offer a more universal treatment but are incapable of predicting signal amplitudes as in the analytic theory described here.

II. THEORY

Assuming the quantum system of Fig. 1, appropriate for the Pr^{3+} ion, the Raman heterodyne beat signal S for the three states indicated obeys the relationship[3]

$$S=a\,|\,E_0\,|^2 H_{\rm rf}(\rho_{22}^0-\rho_{11}^0)\mu_{12}\mu_{23}\mu_{31} \times \mathrm{Re}w(\bar{\Delta}_E/\sigma_E)\mathrm{Im}(w[(\bar{\Delta}_H+i\gamma_{12})/\sigma_H]e^{i\omega t}) \quad (2.1)$$

with

$$a=\pi^2 k_E LN/(\sigma_E\sigma_H\hbar^2)\ .$$

Here, ω is the rf or heterodyne beat frequency and $\mu_{12}\mu_{23}\mu_{31}$ is the transition-matrix product (1.1). The optical and rf field amplitudes are E_0 and $H_{\rm rf}$, k_E is the optical wave vector, L is the sample length, N is the impurity-ion number density, $\rho_{22}^0-\rho_{11}^0$ is the ground-state population difference, and the line-shape function is

$$w(z)=(i/\pi)\int_{-\infty}^{\infty}(e^{-t^2})/(z-t)dt,\quad \mathrm{Im}z>0\ .$$

Finally, $\bar{\Delta}_E$ and $\bar{\Delta}_H$ are the optical and rf tuning parameters, σ_E and σ_H are the corresponding inhomogeneous linewidths, and γ_{12} is the rf homogeneous linewidth.

The purpose of this section is to develop expressions based on (2.1) or more simply (1.1) that reveal interference through the contribution of different nuclear sites or, in the case of a single site, the contribution of different Zeeman-split transitions.

The relevant transition-matrix elements of (2.1) are

$$\mu_{12}=\langle 1\,|\,\mu\,|\,2\rangle\ , \quad (2.2a)$$

$$\mu_{23}=\langle 2\,|\,\mu'\,|\,3\rangle=\langle\varphi_g\,|\,\mu'\,|\,\varphi_e\rangle\langle m_2\,|\,m_3\rangle\ , \quad (2.2b)$$

$$\mu_{31}=\langle 3\,|\,\mu'\,|\,1\rangle=\langle\varphi_e\,|\,\mu'\,|\,\varphi_g\rangle\langle m_3\,|\,m_1\rangle\ , \quad (2.2c)$$

where the magnetic dipole operator

$$\mu_i=\gamma_i\hbar I_i\ ,\quad i=x,y,z \quad (2.3)$$

μ' is an electric or magnetic dipole operator for an optical transition with moment

$$p=\langle\varphi_g\,|\,\mu'\,|\,\varphi_e\rangle\ , \quad (2.4)$$

and we assume that the electronic $|\,\varphi\rangle$ and nuclear $|\,m\rangle$ wave functions are separable in the ground (g) and excited (e) electronic states.

To evaluate these transition-matrix elements, we write the $Pr^{3+}(I=\frac{5}{2})$ nuclear quadrupole and Zeeman Hamiltonian[6-8] as

$$\mathscr{H}=D[I_z^2-I(I+1)/3]+E(I_x^2-I_y^2) -\hbar H_0(\gamma_x I_x\sin\theta\cos\varphi +\gamma_y I_y\sin\theta\sin\varphi+\gamma_z I_z\cos\theta)\ , \quad (2.5)$$

which applies for a nuclear spin with angular momentum $I\hbar$. Here, a static external magnetic field H_0 has polar coordinates (θ,φ) with respect to the principal nuclear Z axis of the quadrupole tensor. In general, the nuclear axes for ground ($^3H_4$) and excited ($^1D_2$) electronic states will be incongruent and the gyromagnetic ratios $\gamma_{x,y,z}$ and the quadrupole parameters D and E for these two electronic states will differ also. We shall see that site interference appears only when the nuclear axes are incongruent.

For the case of a nonaxial electronic field gradient at the Pr nucleus, the nuclear quadrupole eigenvectors[8,9]

$$|\,\pm m_i\,\rangle=\sum_m a_m^{(i)}\psi_{\pm m}\ ,\quad m=\tfrac{5}{2},\tfrac{1}{2},-\tfrac{3}{2} \quad (2.6)$$

are mixed in the axial basis set $\psi_{\pm m}$ [corresponding to $E=0$ in Eq. (2.5)] where the quadrupole Hamiltonian connects only states differing by $\Delta m=\pm 2$ and the upper and lower signs express a twofold degeneracy in zero magnetic field. Here, the mixing coefficients a_m are symmetric in the sign of m such that $a_m=a_{-m}$. In zero magnetic field, the eigenvectors of the three states are then

$$|\,\pm m_1\,\rangle=\sum_m a_m\psi_{\pm m}\ , \quad (2.7)$$

$$|\,\pm m_2\,\rangle=\sum_m b_m\psi_{\mp m}\ , \quad (2.8)$$

$$|\,\pm m_3'\,\rangle=\sum_m c_m\psi_{\pm m}\ , \quad (2.9)$$

with

$$m=\tfrac{5}{2},\tfrac{1}{2},\text{ and }-\tfrac{3}{2}\ . \quad (2.10)$$

The sign of (2.8) is reversed for convenience to emphasize later that the $\Delta m=\pm 1$ magnetic dipole transition $1\rightarrow 2$ is allowed, even when the state is pure.

A second mixing effect occurs in the excited $|\,m_3'\,\rangle$ state when its nuclear axes are incongruent with those of the ground state. For $|\,m_3'\,\rangle$ to be represented in the same basis set as the ground-state wave functions (2.7) and (2.8), we perform a Eulerian transformation $P(\alpha,\beta,\gamma)$ on (2.9),

$$|\,\pm m_3\,\rangle=P(\alpha,\beta,\gamma)\sum_m c_m\psi_{\pm m} =\sum_{m,m'} c_m\psi_{m'}D^{(j)}(\alpha,\beta,\gamma)_{m'\pm m}\ , \quad (2.11)$$

$$m\{=\tfrac{5}{2},\tfrac{1}{2},-\tfrac{3}{2}\}\text{ and }m'\{=\pm\tfrac{5}{2},\pm\tfrac{1}{2},\mp\tfrac{3}{2}\}\ .$$

The general angular momentum transformation matrix[10] for Eulerian rotations (α,β,γ) about a space-fixed right-hand coordinate system (x,y,z), the principal ground-state quadrupole axes, is

$$[D^{(j)}(\alpha,\beta,\gamma)]_{m'm}=e^{-im'\alpha}e^{-im\gamma}\sum_k \frac{(-1)^k[(j+m)!(j-m)!(j+m')!(j-m')!]^{1/2}}{k!(j+m-k)!(j-m'-k)!(k+m'-m)!}$$
$$\times[\cos(\beta/2)]^{2j-2k-m'+m}[-\sin(\beta/2)]^{2k+m'-m}\ , \tag{2.12}$$

where $j\hbar$ is the total angular momentum. The matrix elements (2.12) for the special case of $j=\frac{5}{2}$ are given in Table I.

The third and final mixing effect occurs upon application of a static magnetic field H_0 that lifts the twofold degeneracy of $|\pm m_i\rangle$ in (2.7)–(2.9). Treating the Zeeman interaction as a perturbation on the quadrupolar terms in (2.5), the Zeeman-induced frequency shift[8] of this 2×2 eigenvalue problem is

$$\omega_{\pm m_i}=\pm(H_0/2)[(\gamma_z A_i\cos\theta)^2+(\gamma_y B_i\sin\theta\sin\varphi)^2$$
$$+(\gamma_x C_i\sin\theta\cos\varphi)^2]^{1/2}\ , \tag{2.13}$$

and for $i=1$,

$$A_1=5a_{5/2}^2+a_{1/2}^2-3a_{3/2}^2\ ,$$
$$B_1=2\sqrt{5}a_{5/2}a_{3/2}-4\sqrt{2}a_{1/2}a_{3/2}+3a_{1/2}^2\ , \tag{2.14}$$
$$C_1=2\sqrt{5}a_{5/2}a_{3/2}+4\sqrt{2}a_{1/2}a_{3/2}+3a_{1/2}^2\ .$$

For $i=2$ or 3, the above coefficients a_m are to be replaced by b_m or c_m, respectively.

The corresponding eigenvectors display mixing of the basis states (2.7), (2.8), and (2.11) of the form

$$|\pm\tilde{m}_i\rangle=\cos\alpha_i\,|\pm m_i\rangle\pm e^{\mp i\xi_i}\sin\alpha_i\,|\mp m_i\rangle\ , \tag{2.15}$$

where $i=\sqrt{-1}$ in the exponent and is a subscript elsewhere,

$$\tan(2\alpha_i)=[(B_i\gamma_y\sin\varphi)^2$$
$$+(C_i\gamma_x\cos\varphi)^2]^{1/2}\tan\theta/(A_i\gamma_z)\ , \tag{2.16}$$
$$\tan\xi_i=(\gamma_y B_i/\gamma_x C_i)\tan\varphi\ . \tag{2.17}$$

The resulting eigenvectors are

$$|\pm\tilde{m}_1\rangle=\sum_m a_m(\cos\alpha_1\psi_{\pm m}\pm e^{\mp i\xi_1}\sin\alpha_1\psi_{\mp m})\ ,$$
$$|\pm\tilde{m}_2\rangle=\sum_m b_m(\cos\alpha_2\psi_{\mp m}\mp e^{\pm i\xi_2}\sin\alpha_2\psi_{\pm m})\ , \tag{2.18}$$
$$|\pm\tilde{m}_3\rangle=\sum_{n,m} c_m\psi_n(\cos\alpha_3 D_{n,\pm m}\pm e^{\mp i\xi_3}\sin\alpha_3 D_{n,\mp m})\ ,$$
$$m\{=\tfrac{5}{2},\tfrac{1}{2},-\tfrac{3}{2}\}\text{ and }n\{\pm\tfrac{5}{2},\pm\tfrac{3}{2},\pm\tfrac{1}{2}\}\ .$$

Now that all the wave functions are determined, the three transition-matrix elements (2.2) are readily calculated. Considering only the case of upper signs in (2.18), the explicit expressions for (2.2) become

$$\mu_{12}=\sum_{m,m'}\gamma_i\hbar a_m b_{m'}(\cos\alpha_1\cos\alpha_2\langle m\,|\,I_i\,|\,-m'\rangle+e^{i\xi_1}\sin\alpha_1\cos\alpha_2\langle -m\,|\,I_i\,|\,-m'\rangle$$
$$-e^{i\xi_2}\cos\alpha_1\sin\alpha_2\langle m\,|\,I_i\,|\,m'\rangle-e^{i(\xi_1+\xi_2)}\sin\alpha_1\sin\alpha_2\langle -m\,|\,I_i\,|\,m'\rangle)\ , \tag{2.19}$$
$$i\{=x,y,z\}\text{ and }m,m'\{=\tfrac{5}{2},\tfrac{1}{2},-\tfrac{3}{2}\}\ ,$$

$$\mu_{23}=\sum_{m,m'}pb_m c_{m'}(\cos\alpha_2\cos\alpha_3 D_{-mm'}-e^{-i\xi_2}\sin\alpha_2\cos\alpha_3 D_{mm'}$$
$$+e^{-i\xi_3}\cos\alpha_2\sin\alpha_3 D_{-m-m'}-e^{-i(\xi_2+\xi_3)}\sin\alpha_2\sin\alpha_3 D_{m-m'})\ ,\quad m,m'\{=\tfrac{5}{2},\tfrac{1}{2},-\tfrac{3}{2}\}\ , \tag{2.20}$$

$$\mu_{31}=\sum_{m,m'}p^* c_m a_{m'}(\cos\alpha_3\cos\alpha_1 D^*_{m'm}+e^{i\xi_3}\sin\alpha_3\cos\alpha_1 D^*_{m'-m}$$
$$+e^{-i\xi_1}\cos\alpha_3\sin\alpha_1 D^*_{-m'm}+e^{i(\xi_3-\xi_1)}\sin\alpha_3\sin\alpha_1 D^*_{-m'-m})\ ,\quad m,m'\{=\tfrac{5}{2},\tfrac{1}{2},-\tfrac{3}{2}\}\ . \tag{2.21}$$

The Raman heterodyne signal S [Eq. (1.1)] follows by taking the triple product of (2.19)–(2.21). Since the relative orientation of ground- and excited-state nuclear quadrupole axes affects the elements μ_{23} and μ_{31}, two inequivalent sites, for example, can generate Raman signals S of different phase that interfere. On the other hand, when the rf field is properly oriented, Zeeman-split rf transitions can show interference within a single site.

III. Pr^{3+}:$YAlO_3$

A. Site interference

A clear example[1] of site interference can be found in the impurity-ion crystal Pr^{3+}:$YAlO_3$. The Pr^{3+} ions substitute for the Y^{3+} ions in two inequivalent sites of point symmetry C_{1h}. As can be seen in Fig. 3, this requires that two principal nuclear quadrupole axes (Z,Y) lie in a plane

TABLE I. D matrix for $j=\frac{5}{2}$.

$[D^{(5/2)}(\alpha,\beta,\gamma)]_{m'm}=e^{-i(m'\alpha+m\gamma)}d_{m'm}(\beta)$

$d_{5/2,5/2}=c^5$
$d_{5/2,3/2}=-\sqrt{5}c^4s$
$d_{5/2,1/2}=\sqrt{10}c^3s^2$
$d_{5/2,-1/2}=-\sqrt{10}c^2s^3$
$d_{5/2,-3/2}=\sqrt{5}cs^4$
$d_{5/2,-5/2}=-s^5$
$d_{3/2,3/2}=c^5-4c^3s^2$
$d_{3/2,1/2}=-2\sqrt{2}c^4s+3\sqrt{2}c^2s^3$
$d_{3/2,-1/2}=3\sqrt{2}c^3s^2-2\sqrt{2}cs^4$
$d_{3/2,-3/2}=-4c^2s^3+s^5$
$d_{1/2,1/2}=c^5-6c^3s^2+3cs^4$
$d_{1/2,-1/2}=-3c^4s+6c^2s^3-s^5$
$c\equiv\cos(\beta/2)$, $s\equiv\sin(\beta/2)$
$d_{m'm}=(-1)^{m'-m}d_{-m'-m}, d_{m'm}=(-1)^{m'-m}d_{mm'}$, etc.

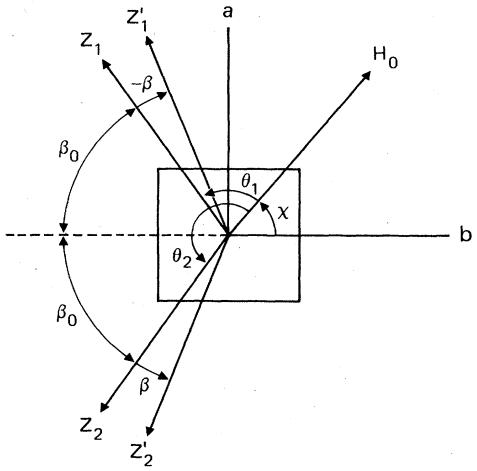

FIG. 3. Principal nuclear quadrupole Z axis of Pr lies in the crystal a-b plane of $YAlO_3$ and perpendicular to the crystal c axis ($=X$ axis). The two inequivalent sites for $^3H_4(Z_{1,2})$ or $^1D_2(Z'_{1,2})$ make equal angles with the b axis. The static magnetic field H_0 is in the a-b plane and deviates from the b axis by the angle χ.

of symmetry, the a-b plane, while the third axis (X) points along the c axis. Figure 3 therefore shows that the principal Z axes for the two inequivalent sites make equal angles with the b axis in the ground electronic state $^3H_4(Z_{1,2})$ and in the excited state $^1D_2(Z'_{1,2})$ where the angles $\pm\beta$ mark the degree of incongruence.

Equations (2.19)–(2.21) simplify when we allow (a) $\mathbf{H}_0\perp c$ axis so that $\varphi=\pi/2$ and $\xi_i=\pi/2$ ($i=1,2,3$) in (2.17) and (b) the Eulerian angles are set equal to $(\alpha,\beta,\gamma)=(\pi/2,\beta,-\pi/2)$. We thus obtain

$$\mu_{12}=\sum_{m,m'}\gamma_x\hbar a_m b_{m'}\langle m\,|\,I_x\,|\,-m'\rangle\cos(\alpha_1-\alpha_2)\,, \tag{3.1}$$

$$\mu_{23}=\sum_{m,m'}pb_m c_{m'}[D_{-mm'}(\beta)\cos(\alpha_2-\alpha_3) +iD_{mm'}(\beta)\sin(\alpha_2-\alpha_3)]\,, \tag{3.2}$$

$$\mu_{31}=\sum_{m,m'}p^*c_m a_{m'}[D_{m'm}(\beta)\cos(\alpha_3-\alpha_1) +iD_{m'-m}(\beta)\sin(\alpha_3-\alpha_1)]\,, \tag{3.3}$$

where

$$m,m'\{=\tfrac{5}{2},\tfrac{1}{2},-\tfrac{3}{2}\}\,, \tag{3.4}$$

and where we have used the relation

$$D_{mn}(\beta)=D_{-m-n}(\beta)\,,$$

appropriate to this particular case (see Table I).

It is now possible to predict how the Raman heterodyne signal

$$S\sim\mu_{12}\mu_{23}\mu_{31} \tag{1.1}$$

behaves for site interference. In explicit form, we write

$$S=\sum_{m_1,m_2,\ldots,m_6=\frac{5}{2},\frac{1}{2},-\frac{3}{2}}c(\gamma_x)\langle m_1\,|\,I_x\,|\,-m_2\rangle\cos(\alpha_1-\alpha_2)\,, \tag{3.5}$$

$$c(\gamma_x)=\gamma_x\hbar\,|\,p\,|^2a_{m_1}b_{m_2}b_{m_3}c_{m_4}c_{m_5}a_{m_6}[D_{-m_3m_4}(\beta)\cos(\alpha_2-\alpha_3)+iD_{m_3m_4}(\beta)\sin(\alpha_2-\alpha_3)] \times[D_{m_5m_6}(\beta)\cos(\alpha_1-\alpha_3)-iD_{-m_5m_6}(\beta)\sin(\alpha_1-\alpha_3)]\,. \tag{3.6}$$

From Table I, we see that

$$D_{mm'}(-\beta)=D_{mm'}(\beta)\,, \tag{3.7}$$

$$D_{-mm'}(-\beta)=-D_{-mm'}(\beta) \tag{3.8}$$

applies because of the restriction (3.4).

For the case of zero static field ($H_0=0$), each α_i is zero and (3.6) reduces to the form

$$c(\gamma_x)\sim D_{-m_3m_4}(\beta)D_{m_5m_6}(\beta)\,, \tag{3.9}$$

which implies using (3.7) and (3.8) that the signals of the two inequivalent sites obey

$$S_1(\beta)=-S_2(-\beta)\,. \tag{3.10}$$

In other words, since $D_{-m_3m_4}(\beta)$ is odd in β and $D_{m_5m_6}(\beta)$ is even in β, the two sites of Fig. 3 generate Raman heterodyne beat signals of opposite sign and thus interfere destructively with $H_0=0$ when the Zeeman levels are degenerate.

For a nonzero static field H_0 applied either along the crystal a axis ($\theta_1=\pi-\theta_2$) or b axis ($\theta_1=-\theta_2$), we see

from (2.16) that the two sites exhibit a sign reversal in α_i. This fact and the inclusion of (3.7) and (3.8) in (3.6) again yields (3.10) and interference. However, as the field angle varies the signals separate as in Fig. 2 for $\chi=33.6°$ where the sign reversal in the two signals $S_{1,2}$ is obvious at elevated field strengths. Furthermore, it is important to realize that when the principal Z axes of Fig. 3 are congruent, making $\beta=0$, mixing in the excited state (2.11) vanishes and the Raman signals vanish. Some other special cases also show the behavior (3.10), but the parity problem for an arbitrary field angle χ is not yet solved and probably requires numerical calculation.

B. Zeeman interference

In the previous section, site interference was demonstrated for the case where (i) the rf magnetic field H_{rf} is applied along the X (c) axis and (ii) the three states selected in (2.18) are $|+\tilde{m}_1\rangle$, $|+\tilde{m}_2\rangle$, and $|+\tilde{m}_3\rangle$. Similarly, if we had selected $|-\tilde{m}_1\rangle$, $|-\tilde{m}_2\rangle$, and $|-\tilde{m}_3\rangle$ instead, the same site interference would prevail. We now repeat the above calculation beginning with (2.18) by (a) allowing H_{rf} to be oriented in the plane of the Y and Z principal axes to break the site symmetry and (b) selecting a single site with a conjugate pair of states $|\tilde{m}_1\rangle$, $|\tilde{m}_2\rangle$, $|\tilde{m}_3\rangle$; and $|-\tilde{m}_1\rangle$, $|-\tilde{m}_2\rangle$, $|-\tilde{m}_3\rangle$. The details of this calculation are given in Appendix A and yield

$$S_{\pm}=\sum c(\gamma_x)\langle m_1|I_x|-m_2\rangle\cos(\alpha_1-\alpha_2)\ ,\quad \mathbf{H}_{rf}||X \tag{3.11}$$

$$S_{\pm}=\pm\sum c(\gamma_y)\langle m_1|I_y|-m_2\rangle\cos(\alpha_1+\alpha_2)\ ,\quad \mathbf{H}_{rf}||Y \tag{3.12}$$

$$S_{\pm}=\mp\sum c(\gamma_z)im_1\delta_{m_1m_2}\sin(\alpha_1+\alpha_2)\ ,\quad \mathbf{H}_{rf}||Z \tag{3.13}$$

where $c(\gamma_i)$ is defined by (3.6) with γ_i ($i=x$, y, or z), the sums extend our $m_1, m_2, \ldots, m_6\{=\frac{5}{2},\frac{1}{2},-\frac{3}{2}\}$, and δ is the Kronecker delta function. Thus, for $\mathbf{H}_{rf}||X$, the two Zeeman-split transitions $\tilde{m}_i\rightarrow\tilde{m}_j$ and $-\tilde{m}_i\rightarrow-\tilde{m}_j$ are of the same sign, whereas they are of opposite sign for (3.12) and (3.13). An experimental example of Zeeman interference is shown in Fig. 4, and it is clear that the signal will vanish because of interference only when $H_0=0$.

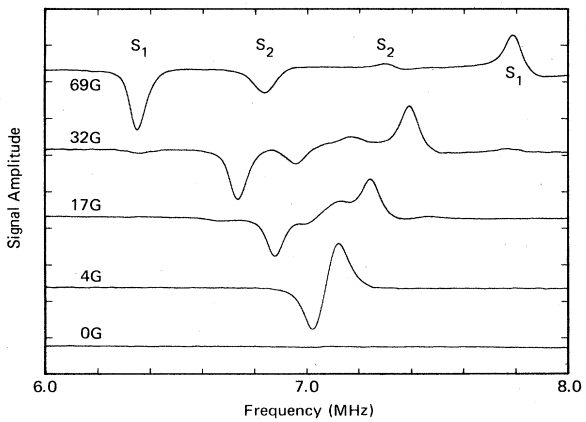

FIG. 4. Observed Raman heterodyne beat spectrum in absorption for the $^3H_4|\pm\frac{3}{2}\rangle\leftrightarrow|\pm\frac{1}{2}\rangle$ transitions of 0.1 at. % Pr^{3+}:$YAlO_3$ as a function of H_0 ($\chi=33.6°$) where $\mathbf{H}_{rf}\perp c$ axis. Zeeman interference appears in each of the two sites $S_{1,2}$ as a pair of signals of opposite sign. Interference is complete at $H_0=0$.

In summary, the signal always vanishes at $H_0=0$ regardless of the rf orientation: (i) when $\mathbf{H}_{rf}||X$ due to site interference and (ii) when $\mathbf{H}_{rf}||Y$ or $\mathbf{H}_{rf}||Z$ due to Zeeman interference. It is therefore concluded that the signal vanishes for $H_0=0$ for any orientation of the rf field since the resulting signal is a linear combination of the three directions.

C. Experiments

Raman heterodyne signals are observed with the apparatus described previously.[1,2] A Coherent 599 single mode, linearly polarized cw dye laser oscillating in the locked mode with a linewidth of $\sim$4 MHz at 6107 Å excited the Pr^{3+} $^3H_4\rightarrow{}^1D_2$ transition by propagating along the c axis of a 0.1 at. % Pr^{3+}:$YAlO_3$ crystal ($5\times5\times1.1$ mm^3). Since the optical dipole matrix elements are equal in the Y and Z directions,[11] the signals are independent of the angle of polarization—a situation that contrasts sharply with Pr^{3+}:LaF_3.[12] The laser beam of 10—20 mW power was focused to a diameter of 50—100 μm in the sample. The crystal was mounted in a small pair of Helmholtz coils with $\mathbf{H}_{rf}||c$ axis for site interference or $\mathbf{H}_{rf}\perp c$ axis for Zeeman interference, and together were immersed in a liquid-helium cryostat at 1.7 K.

To determine the Zeeman tuning behavior of the two sites, a static external field H_0 that could be rotated in a plane perpendicular to the c axis was supplied by two external orthogonal pairs of Helmholtz coils. Radiofrequency fields up to 0.3 G in the range $\omega/2\pi=0.7$—20 MHz excited the Pr^{3+} hyperfine transitions

$$|\pm\tfrac{3}{2}\rangle\rightarrow|\pm\tfrac{5}{2}\rangle\ ,\quad |\pm\tfrac{1}{2}\rangle\rightarrow|\pm\tfrac{3}{2}\rangle \tag{3.14}$$

in both the $^3H_4$ and $^1D_2$ states.

The forward-scattered laser light was incident on an EG&G model FND-100 photodiode which registered the Raman heterodyne beat. To improve the signal-to-noise ratio, the heterodyne beat signal was averaged with a Data Precision 6000 waveform analyzer which utilizes a 100-kHz 14-bit digitizer with typically 2^8 sweeps for the $^3H_4$ ground-state signal. Longer averaging times were required for the $^1D_2$ excited state since the resonant frequencies (0.9, 1.6 MHz) fall within the dye laser amplitude noise bandwidth.

TABLE II. Zero-field quadrupole splittings f and inhomogeneous linewidths Δf (full width of half maximum) of Pr^{3+}:$YAlO_3$.

	f (MHz)	Δf(kHz)
$^3H_4(\pm\frac{1}{2}\leftrightarrow\pm\frac{3}{2})$	7.062±0.005	55±6
$^3H_4(\pm\frac{3}{2}\leftrightarrow\pm\frac{5}{2})$	14.108±0.009	94.5±6
$^1D_2(\pm\frac{1}{2}\leftrightarrow\pm\frac{3}{2})$	0.922±0.010	14±3
$^1D_2(\pm\frac{3}{2}\leftrightarrow\pm\frac{5}{2})$	1.569±0.005	13.5±2

TABLE III. Quadrupole parameters $|D|$ and $|E|$, asymmetry parameter η, and the gyromagnetic ratios of Pr^{3+}:$YAlO_3$.

	$\lvert D\rvert$ (MHz)	$\lvert E\rvert$ (MHz)	η	$\gamma_z/2\pi$ (kHz/G)	$\gamma_y/2\pi$ (kHz/G)
$^3H_4$	3.5276	0.035	0.030	11.785	2.43
$^1D_2$	0.4026	0.050	0.375	1.570	1.48

1. *Quadrupole splittings and linewidths*

The quadrupole splittings and inhomogeneous linewidths determined here are summarized in Table II where the line centers are in agreement with earlier work[13] and in some cases are more precise. As a comparison, the homogeneous linewidth from Raman heterodyne detected spin echoes decreases from ~ 5 to 2 kHz as H_0 increases from 1 to 18 G. Because of site interference at $H_0=0$, zero-field line centers were determined from the Zeeman splittings which were fit with an eigenvalue expression for the complete quadrupole-Zeeman Hamiltonian (2.5). The resulting quadrupole parameters D and E, the asymmetry parameter $\eta=|3E/D|$, and the gyromagnetic ratios are summarized in Table III. The corresponding eigenvector amplitudes are given in Table IV and the Zeeman parameters A, B, C in Table V.

2. *Site interference*

As already mentioned, Fig. 2 is a clear example of site interference. Each site displays two strong transitions $^3H_4|+\tilde{\frac{1}{2}}\rangle\rightarrow|+\tilde{\frac{3}{2}}\rangle$ and $^3H_4|-\tilde{\frac{1}{2}}\rangle\rightarrow|-\tilde{\frac{3}{2}}\rangle$ where the signs corresponding to the two sites are reversed, in agreement with (3.10). The weaker transitions $^3H_4|+\tilde{\frac{1}{2}}\rangle\rightarrow|-\tilde{\frac{3}{2}}\rangle$ and $^3H_4|-\tilde{\frac{1}{2}}\rangle\rightarrow|+\tilde{\frac{3}{2}}\rangle$ have been observed also but at higher gain or higher field strengths. Here, the case of $\mathbf{H}_{rf}||c$ axis has an amplitude of 0.3 G while H_0 lies in the a-b plane at an angle $\chi=33.6°$ to the b axis (see Fig. 3). For $H_0\sim 0$, the site interference effect occurs because of the near cancellation of S_1 and S_2. At $H_0=4$ G, the anomalous second-derivative–like line shape observed previously appears.[1,2] Above 32 G, all four strong lines are fully resolved and exhibit sign reversal in the two sites.

Site interference persists also for $H_0\neq 0$ when H_0 is oriented either along the crystal a or b axis so that the site symmetry is unaffected. In fact, when the orientation of H_0 is varied, the positive and negative signals "collide" and exactly cancel at the symmetry points $H_0||a$ and $H_0||b$. This behavior is illustrated in the normalized angular Zeeman spectrum of Fig. 5, shown as a function of the angle χ that H_0 makes with the crystal b axis and for the transitions (a) $^3H_4|\pm\frac{3}{2}\rangle\rightarrow|\pm\frac{1}{2}\rangle$ and (b) $^1D_2|\pm\frac{5}{2}\rangle\rightarrow|\pm\frac{3}{2}\rangle$, four transitions for each site. The experimental points fall nicely on the theoretical fit for site S_1 (solid curve) and site S_2 (dashed curve). Interferences are evident when the static field ($H_0=50$ G) is oriented either parallel to the b axis ($\chi=0$) or to the a axis ($\chi=90°$). From this figure, we conclude that the principal Z axis of the $^3H_4$ and $^1D_2$ states are located at angles

$$\beta_0=56.4°(^3H)\ ,\quad \beta_0+\beta=69.2°(^1D_2) \tag{3.15}$$

off the b axis (see Fig. 3), the two sites for each state $Z_{1,2}$ and $Z'_{1,2}$ being oriented symmetrically about the b axis. The ground-state angle agrees well with that of Erickson[11]

TABLE IV. Amplitudes of eigenstates $|\pm m\rangle=a_{5/2}\psi_{\pm 5/2}+a_{1/2}\psi_{\pm 1/2}+a_{3/2}\psi_{\mp 3/2}$.

		$\psi_{\pm 5/2}$	$\psi_{\pm 1/2}$	$\psi_{\mp 3/2}$
Pr^{3+}:$YAlO_3$				
ground state $^3H_4$	$\lvert\pm\frac{5}{2}\rangle$	0.999 99	0.005 20	0.000 05
	$\lvert\pm\frac{1}{2}\rangle$	−0.005 20	0.999 77	−0.020 91
	$\lvert\mp\frac{3}{2}\rangle$	−0.000 16	0.020 91	0.999 78
excited state $^1D_2$	$\lvert\pm\frac{5}{2}\rangle$	0.997 77	0.066 18	0.008 71
	$\lvert\pm\frac{1}{2}\rangle$	−0.062 21	0.969 19	−0.238 32
	$\lvert\mp\frac{3}{2}\rangle$	−0.024 22	0.237 24	0.971 15
Pr^{3+}:LaF_3[a]				
ground state $^3H_4$	$\lvert\pm\frac{5}{2}\rangle$	0.999 82	0.019 02	0.000 73
	$\lvert\pm\frac{1}{2}\rangle$	−0.018 91	0.996 95	−0.075 75
	$\lvert\mp\frac{3}{2}\rangle$	−0.002 17	0.075 73	0.997 13
excited state $^1D_2$	$\lvert\pm\frac{5}{2}\rangle$	0.991 54	0.126 13	0.030 76
	$\lvert\pm\frac{1}{2}\rangle$	−0.105 88	0.922 75	−0.370 58
	$\lvert\mp\frac{3}{2}\rangle$	−0.075 12	0.364 19	0.928 29

[a]Taken from Ref. 3.

TABLE V. Zeeman parameters A, B, C of Eq. (2.14). The subscripts i of A_i, B_i, C_i refer to the eigenvectors $|i\rangle$ of TABLE IV.

	$^3H_4$	$^1D_2$
Pr^{3+}:$YAlO_3$		
$A_{5/2}$	4.999 93	4.981 88
$B_{5/2}$	0.000 30	0.048 74
$C_{5/2}$	0.000 31	0.055 27
$A_{3/2}$	−2.998 24	−2.770 18
$B_{3/2}$	−0.117 66	−1.239 66
$C_{3/2}$	0.118 86	1.366 97
$A_{1/2}$	0.998 36	0.788 29
$B_{1/2}$	3.117 36	4.190 90
$C_{1/2}$	2.880 85	1.577 69
Pr^{3+}:LaF_3		
$A_{5/2}$	4.998 56	4.928 83
$B_{5/2}$	0.004 27	0.162 18
$C_{5/2}$	0.004 43	0.206 07
$A_{3/2}$	−2.977 05	−2.424 32
$B_{3/2}$	−0.419 64	−1.826 39
$C_{3/2}$	0.434 69	1.998 48
$A_{1/2}$	0.978 48	0.495 53
$B_{1/2}$	3.415 33	4.664 25
$C_{1/2}$	2.560 93	0.795 50

while the excited-state angle, which has been difficult to obtain, is a new determination. Thus, ground- and excited-state Z axes are rotated by $\pm 12.8°$. Similar measurements for $^1D_2 \mid \pm\frac{3}{2}\rangle \rightarrow \mid \pm\frac{1}{2}\rangle$ gave less precise results than Fig. 5 because of a poorer signal-to-noise ratio.

3. Zeeman interference

Figure 4 shows the Zeeman-interference effect for the $^3H_4 \mid \pm\frac{3}{2}\rangle \rightarrow \mid \pm\frac{1}{2}\rangle$ transition with the H_{rf} field in the crystal a-b plane while H_0 is at an angle $\chi = 33.6°$. The Zeeman spectrum for each site $S_{1,2}$ appears as a conjugate pair of transitions $|\tilde{\tfrac{1}{2}}\rangle \rightarrow |\tilde{\tfrac{3}{2}}\rangle$ and $|-\tilde{\tfrac{1}{2}}\rangle \rightarrow |-\tilde{\tfrac{3}{2}}\rangle$ which are reversed in sign, the splittings being different in the two sites because of the difference in angles $Z_{1,2} \nparallel H_0$. At zero static field, the signal vanishes because the interference is complete. At nonzero fields, the Zeeman pattern reveals its inversion symmetry in contrast to the mirror symmetry of site interference of Fig. 2. Therefore, Eqs. (3.12) and (3.13) are verified and (3.11) follows the site interference measurements.

IV. Pr^{3+}:LaF_3

A. Zeeman spectra

Compared to the Pr^{3+}:$YAlO_3$ crystal, the Zeeman spectrum of the Pr^{3+}:LaF_3 crystal is much more difficult to analyze for the following reasons: (i) This crystal has six sites,[14] and because they are degenerate in pairs, three inequivalent sites participate in the signal. (ii) Each site exhibits an optical polarization dependence where the interference pattern changes dramatically as the polarization angle is varied. (iii) The inhomogeneous linewidths of both ground and excited states are almost three times as broad as the Pr^{3+}:$YAlO_3$ crystal and thus a higher static field is required to resolve all the Zeeman components. Furthermore, Sec. II assumes that the Zeeman effect is a perturbation, which may no longer be valid. Nevertheless, the interference effect appears as an intrinsic property of Raman heterodyne detection.

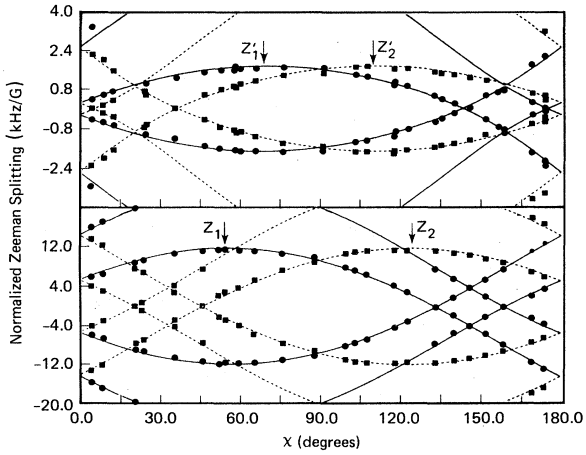

FIG. 5. Zeeman absorption spectrum of the excited-state $^1D_2 \mid \pm\frac{5}{2}\rangle \leftrightarrow \mid \pm\frac{3}{2}\rangle$ transition (upper curve) and the ground-state $^3H_4 \mid \pm\frac{3}{2}\rangle \rightarrow \mid \pm\frac{1}{2}\rangle$ transition (lower curve) of 0.1 at. % Pr^{3+}:$YAlO_3$ as a function of the angle χ that $H_0 \sim 50$ G makes with the crystal b axis. Experimental points for sites 1 (circles) and 2 (squares). Theoretical curves for sites 1 (solid) and 2 (dashed). The angle $\chi = 20.8°$ locates the Z_2' axis angle $\beta_0 = \pi/2 - \chi = 69.2°$. Four arrows show the locations of the principal axes $Z_{1,2}$ of the ground state and excited state of sites 1 and 2.

In Fig. 6, Zeeman spectra are shown which illustrate

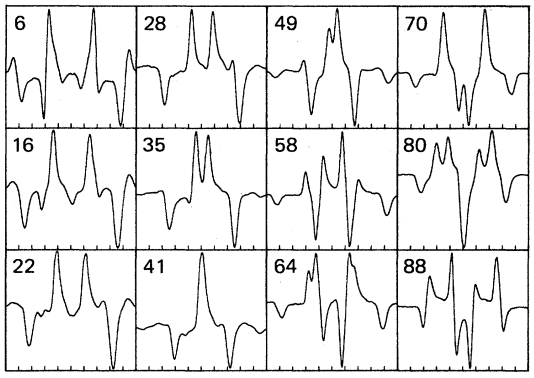

FIG. 6. Zeeman absorption spectra of 1 at. % Pr^{3+}:LaF_3 as a function of orientation of the static magnetic field H_0. Various interference patterns are observed. In each figure, the number represents the angle χ between H_0 and the local C_2 axis and the frequency is swept from 6.5 to 10.5 MHz. Optical polarization was chosen so as to eliminate the contribution of one site.

this complex behavior and where the patterns no longer have the simplicity of Pr^{3+}:$YAlO_3$. The theory is also more complex and while numerical solutions based on the development of Sec. II are feasible, they are not performed here. Instead, this section is more phenomenological than the last section and introduces the observed symmetry properties of the Pr^{3+} hyperfine transitions for $|\pm\frac{3}{2}\rangle \rightarrow |\pm\frac{1}{2}\rangle$ and for $|\pm\frac{5}{2}\rangle \rightarrow |\pm\frac{3}{2}\rangle$, four for each case, as well as the conclusions drawn regarding site orientation in the $^3H_4$ and $^1D_2$ states.

The LaF_3 c axis is the C_3 symmetry axis of the crystal, and the three C_2 site axes perpendicular to it make angles of 120° with one another as in Fig. 8. For each C_2 axis, there are two sites associated with it,[14] and for symmetry to be preserved in a twofold rotation about C_2, one axis (X, Y, or Z) of $^3H_4$ and one of (X', Y', or Z') of $^1D_2$ must be parallel to a C_2 axis. The orientation and assignment of the ground-state axes (X, Y, Z) seem to be well established[14] but the excited-state (X', Y', Z') axes have been more controversial. Reddy and Erickson[14] reported for $^3H_4$ that Y is along C_2 and Z makes an angle of 81.4° with C_3. Whittaker and Hartmann[15] inferred from a photon echo modulation experiment that Z and X' are parallel to a C_2 axis, X and Z' make an angle of 30° with each other, but the location of C_3 relative to X and Z' was unknown. Macfarlane and Shelby[16] concluded from their high-field studies that Y and X' are parallel to C_2, Z is 90° from C_3 and Z' is 20° from C_3.

Our results are presented in Fig. 7 where the Zeeman spectrum for the $^3H_4 |\pm\frac{5}{2}\rangle \rightarrow |\pm\frac{3}{2}\rangle$ and $^1D_2 |\pm\frac{5}{2}\rangle \rightarrow |\pm\frac{3}{2}\rangle$ transitions are plotted against the angle χ that H_0 makes with the local C_2 axis as in Fig. 8. In this work, the laser was tuned to the 5925-Å transition $^3H_4 \rightarrow {}^1D_2$ with the beam propagating along the c axis of a 1 at. % Pr^{3+}:LaF_3 crystal ($4\times5\times3.5$ mm^3). The rf magnetic field was applied parallel to the C_3 axis. The rf transition frequencies and gyromagnetic ratios are published elsewhere.[3] In contrast to Pr^{3+}:$YAlO_3$, only the optical matrix element in the C_2 direction is nonvanishing,[12] and thus, the magnitude of the signal depends on the polarization angle in the case of Pr^{3+}:LaF_3.

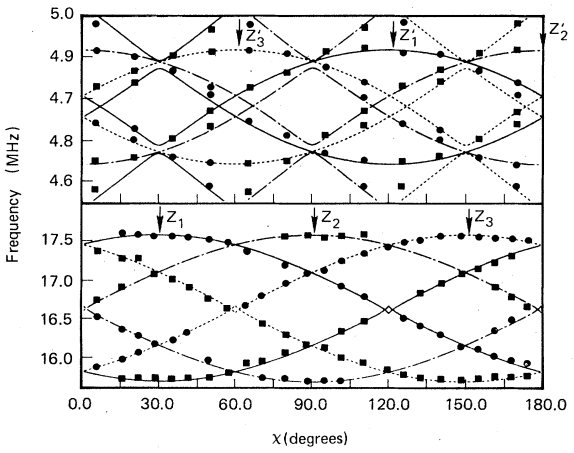

FIG. 7. Zeeman absorption spectra of the ground-state $^3H_4 |\pm\frac{5}{2}\rangle \rightarrow |\pm\frac{3}{2}\rangle$ transition (lower curve) and the excited-state $^1D_2 |\pm\frac{5}{2}\rangle \rightarrow |\pm\frac{3}{2}\rangle$ transition (upper curve) of 1 at. % Pr^{3+}:LaF_3 as a function of the angle χ between H_0 and the local C_2 axis. Experimental points for positive signal (circles) and for negative signal (squares). Theoretical curves for site 1 (solid), site 2 (dot-dash), and site 3 (dashed). Six arrows show the locations of Z axes of the ground state and excited state of sites 1, 2, and 3. $H_0=50$ G in upper figure and 93 G in lower figure.

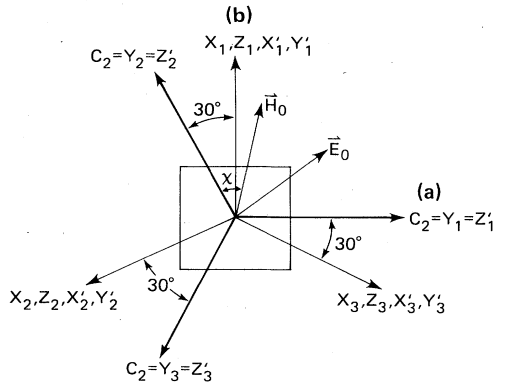

FIG. 8. Three local C_2 axes of Pr^{3+}:LaF_3 make an angle of 120° with one another and lie in the plane perpendicular to the C_3 axis. The ground-state Y and the excited-state Z' axis share the same axis along C_2. The rest of the axes are not in this plane but, when projected onto this plane, are located as shown in the figure. The static magnetic field H_0 and the optical electric field E_0 are also in the same plane.

In Fig. 7, the Z axes for ground and excited states are marked by an arrow and occur at the maximum Zeeman splittings. The theoretical curves for the $^3H_4$ state again use (2.13), where the values[14] $\gamma_x/2\pi=4.98$, $\gamma_y/2\pi=2.53$, and $\gamma_z/2\pi=10.16$ kHz/G and the orientation assignment of (X,Y,Z) agrees perfectly with that of Erickson.[14]

The theoretical fit for the excited $^1D_2$ state utilizes[16] $\gamma'_x/2\pi=3.6$, $\gamma'_y/2\pi=1.9$, and $\gamma'_z/2\pi=2.2$ kHz/G where we have invoked the assignment that Z' is along C_2 and X' is 20° from the c axis. The result that $Z'||C_2$ is also corroborated by the optical polarization dependence. It should be noted that the high-field orientation assignment[16] of the axes (X',Y',Z') is somewhat arbitrary in that the axes could be relabeled while preserving the angles. However, in our low-field measurements, the quadrupole interactions predetermine the coefficients A, B, and C of (2.14) and remove this ambiguity. The excellent fit suggests the correctness of the assignment of these axes (X,Y,Z) and (X',Y',Z') which are summarized in Fig. 8.

B. Interference

The interference behavior of Pr^{3+} in LaF_3 is much more complicated than in $YAlO_3$. Since there are three inequivalent sites with this experimental setup, there is no one-to-one correspondence between different sites and the polarity of the signal. The second complexity comes from the optical polarization dependence of the signal. The contribution of different sites is dependent on the polarization and therefore exact cancellation of the signal is not expected. If the polarization is perpendicular to one of

the C_2 axes, then that site is eliminated from the signal and the other two sites may site-interfere for an appropriate orientation of the static magnetic field. Various interference patterns are observed as a function of H_0 as shown in Fig. 6, where the optical polarization was chosen to eliminate site 1, making sites 2 and 3 interfere.

The parity problem of each site of this crystal is also complex. Two transitions of the ground state and two transitions of the excited state are observed to exhibit different types of parity behavior, which is summarized in Table VI for the case of the rf field parallel to the c axis. For example, for the ground-state ${}^3H_4\,|\pm\tfrac{3}{2}\rangle\rightarrow|\pm\tfrac{1}{2}\rangle$ manifold, Table VI tells us that the spectrum is an even function $\Delta f_0=f-f_0$ with respect to the center frequency f_0, i.e., $|\tfrac{3}{2}\rangle\rightarrow|\tfrac{1}{2}\rangle$ and $|-\tfrac{3}{2}\rangle\rightarrow|-\tfrac{1}{2}\rangle$ have the same sign as do $|\tfrac{3}{2}\rangle\rightarrow|-\tfrac{1}{2}\rangle$ and $|-\tfrac{3}{2}\rangle\rightarrow|\tfrac{1}{2}\rangle$, but other combinations such as $|\tfrac{3}{2}\rangle\rightarrow|-\tfrac{1}{2}\rangle$ and $|-\tfrac{3}{2}\rangle\rightarrow|\tfrac{1}{2}\rangle$ have the opposite sign. These transitions change their sign when the orientation of H_0 is reversed with respect to the Z axis of one site (for $\chi\rightarrow-\chi$), which causes the signal to vanish when H_0 is along the Z axis. Also, the same transitions retain their sign when the direction of H_0 is reversed with respect to the origin.

It is interesting to note that a single site can be excited alone by aligning the rf field parallel to the Z axis of one site and by aligning the optical polarization so that it is perpendicular to a second site. The former inhibits a rf transition in the first site and the latter inhibits an optical transition in the second site. As an example, consider the ${}^3H_4\,|\pm\tfrac{5}{2}\rangle\rightarrow|\pm\tfrac{3}{2}\rangle$ transition. According to Table VI when $\mathbf{H}_{\rm rf}\perp c$ axis, the $|\tfrac{5}{2}\rangle\rightarrow|\tfrac{3}{2}\rangle$ and the $|-\tfrac{5}{2}\rangle\rightarrow|-\tfrac{3}{2}\rangle$ transitions have the same sign and these by far have the highest intensity, the other possible transitions being negligible. Therefore, only two transitions with the same sign contribute to the signal and this becomes the only example of all the measurements discussed in this article which exhibits no interference behavior. The signal is large even when $H_0=0$ and shows a pure Gaussian line shape (see Fig. 9), as observed in our early measurements[2,3] prior to understanding the interference effect.

The theory for this case is quite difficult mainly because of the nuclear axis orientation. The Eulerian angles α, β, and γ are all nonzero and, consequently, the angles θ and φ are very complicated functions of the angle χ in Fig. 8. It is not known yet whether the properties in Table VI are the result of some numerical approximation or are governed by some general symmetry law.

TABLE VI. Observed symmetry properties of Pr^{3+}:LaF_3 for $\mathbf{H}_{\rm rf}||c$ axis.

	Δf_0[a]	$\chi\rightarrow-\chi$	$H_0\rightarrow-H_0$
${}^3H_4(\pm\frac{3}{2}\rightarrow\pm\frac{1}{2})$	Even	Odd	Even
${}^3H_4(\pm\frac{5}{2}\rightarrow\pm\frac{3}{2})$	Odd	Even	Odd
${}^1D_2(\pm\frac{3}{2}\rightarrow\pm\frac{1}{2})$[b]			
${}^1D_2(\pm\frac{5}{2}\rightarrow\pm\frac{3}{2})$	Odd	Odd	Even

[a]For $\mathbf{H}_{\rm rf}\perp c$ axis, interchange even↔odd.
[b]Results are inconclusive because of a low signal-to-noise ratio.

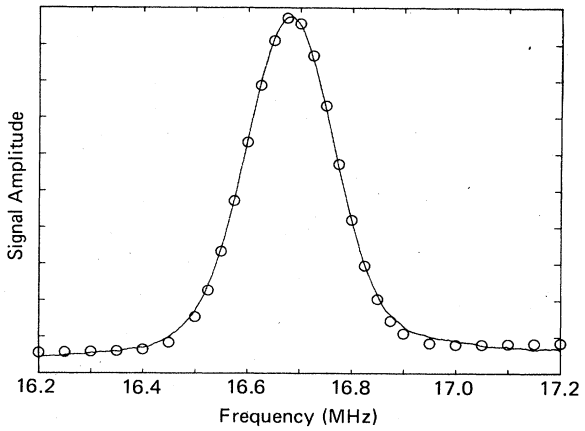

FIG. 9. Raman heterodyne signal of the Pr^{3+}:LaF_3 ground-state $|\pm\frac{5}{2}\rangle\rightarrow|\pm\frac{3}{2}\rangle$ transition for $H_0=0$ G. The rf field is parallel to the Z_1 axis and the optical polarization is parallel to the Z_2 axis (see Fig. 8) showing only one site contributing to the signal. The open circles represent a Gaussian fit.

V. CONCLUSION

One may ask whether the interference effect reported here is unique to Raman heterodyne detection. Certainly other types of optical interference phenomena have been observed in the past. One example is the well-known spin or photon echo effect in a multilevel quantum system.[17] For a four-level case with nearly degenerate ground (1,2) and excited (3,4) states, the echo signal in lowest order takes the form

$$S_{\rm echo}\sim\mu_{24}\mu_{41}\mu_{13}\mu_{32}\ , \tag{5.1}$$

where the four matrix elements connecting these states become active during two-pulse excitation. The linear dependence of each element in (5.1) guarantees a time-dependent interference in the form of a modulated envelope function. However, in this case the interference resides within the molecule itself and is evident only in the time domain. On the other hand, Raman heterodyne interference can be observed either in a steady-state or a coherent transient measurement and within the same (Zeeman-interference) or between different (site-interference) atoms.

In this article, an analytic theory of Raman heterodyne interference was developed which explains in a convincing way the observations of Zeeman and site interference in the impurity-ion crystal Pr^{3+}:$YAlO_3$. The same interference phenomena appear in the Pr^{3+}:LaF_3 crystal but with a dramatic increase in complexity because of a difference

in the number of sites, the crystal symmetry, and the optical polarization dependence. A principal advantage of the interference effect is that it offers a new way of identifying the crystal symmetry, a topic to be discussed further in the accompanying paper. Our discussion has been confined to solids but there is no reason to exclude interference from occurring in gases, and this subject is also under study.

ACKNOWLEDGMENTS

We are indebted to J. Mlynek and N. C. Wong for contributing to the early phases of the quadrupole splitting and linewidth measurements and to K. L. Foster for technical aid. We also thank R. G. DeVoe for stimulating discussions. One of us (E.S.K.) acknowledges partial financial support from IBM. This work was supported in part by the U.S. Office of Naval Research.

APPENDIX A: DERIVATION OF ZEEMAN-INTERFERENCE SIGNAL

We start from the expression (2.18) and obtain each matrix element for two different channels, i.e., $|\tilde{m}_1\rangle\rightarrow|\tilde{m}_2\rangle\rightarrow|\tilde{m}_3\rangle$ and $|-\tilde{m}_1\rangle\rightarrow|-\tilde{m}_2\rangle\rightarrow|-\tilde{m}_3\rangle$. In what follows, repeated indices imply a summation.

The optical transition element $(\mu_{23})_{\pm}$ is calculated as

$$(\mu_{23})_{\pm}\equiv p\langle\pm\tilde{m}_2|\pm\tilde{m}_3\rangle=pb_m c_{m'}(\cos\alpha_2\cos\alpha_3 D_{\mp m\pm m'}\mp e^{\mp i\xi_2}\sin\alpha_2\cos\alpha_3 D_{\pm m\pm m'} \pm e^{\mp i\xi_3}\cos\alpha_2\sin\alpha_3 D_{\mp m\mp m'}-e^{\mp i(\xi_2+\xi_3)}\sin\alpha_2\sin\alpha_3 D_{\pm m\mp m'}) . \tag{A1}$$

Similarly, the other optical transition element $(\mu_{31})_{\pm}$ is

$$(\mu_{31})_{\pm}\equiv p^*\langle\pm\tilde{m}_3|\pm\tilde{m}_1\rangle=p^* a_{m'}c_m(\cos\alpha_3\cos\alpha_1 D^*_{\pm m'\pm m}\pm e^{\pm i\xi_3}\sin\alpha_3\cos\alpha_1 D^*_{\pm m'\mp m} \pm e^{\mp i\xi_1}\cos\alpha_3\sin\alpha_1 D^*_{\mp m'\pm m}+e^{\pm i(\xi_3+\xi_1)}\sin\alpha_3\sin\alpha_1 D^*_{\mp m'\mp m}) . \tag{A2}$$

Notice that the D matrix has the following relations for Pr^{3+}:$YAlO_3$:

$$D^*_{mm'}=D_{mm'},\quad D_{-m-m'}=D_{mm'},\quad D^*_{m-m'}=-D_{m-m'},\quad D_{m-m'}=D_{-mm'}\quad\text{for } m=\{\tfrac{5}{2},\tfrac{1}{2},-\tfrac{3}{2}\} , \tag{A3}$$

which simplifies the above expressions. Further simplification is made assuming the static field H_0 is applied perpendicular to the X axis (in the a-b plane). Then, we get $\varphi=\pi/2$ from the definition (2.5) and, from the definition of ξ_i, (2.17), $\xi_i=\pi/2$ $(i=1,2,3)$. With these considerations, (A1) and (A2) can be rewritten as

$$(\mu_{23})_{\pm}=pb_m c_{m'}[D_{-mm'}\cos(\alpha_2-\alpha_3)+iD_{mm'}\sin(\alpha_2-\alpha_3)] , \tag{A4}$$

$$(\mu_{31})_{\pm}=p^* a_{m'}c_m[D_{m'm}\cos(\alpha_3-\alpha_1)-iD_{m'-m}\sin(\alpha_3-\alpha_1)] . \tag{A5}$$

This means $(\mu_{23})_+=(\mu_{23})_-$ and $(\mu_{31})_+=(\mu_{31})_-$. In other words, optical transition-matrix elements do not change sign for a conjugate pair of transitions, $|\tilde{m}\rangle\rightarrow|\tilde{m}'\rangle$ and $|-\tilde{m}\rangle\rightarrow|-\tilde{m}'\rangle$.

What is the magnetic transition element $(\mu_{12})_{\pm}$? Again from (2.18) we have

$$(\mu_{12})_{\pm}\equiv\gamma_i\hbar\langle\pm\tilde{m}_1|I_i|\pm\tilde{m}_2\rangle=\gamma_i\hbar a_m b_{m'}(\cos\alpha_1\cos\alpha_2\langle\pm m|I_i|\mp m'\rangle+i\sin\alpha_1\cos\alpha_2\langle\mp m|I_i|\mp m'\rangle -i\cos\alpha_1\sin\alpha_2\langle\pm m|I_i|\pm m'\rangle+\sin\alpha_1\sin\alpha_2\langle\mp m|I_i|\pm m'\rangle) \quad\text{for } i\{x,y,\text{ or } z\} , \tag{A6}$$

where $\xi_i=\pi/2$ $(i=1,2,3)$ was again used. Now let us look into this expression in detail for the X, Y, and Z components. For $I=\frac{5}{2}$, I_x, I_y, and I_z are

$$I_X=\frac{1}{2}\begin{pmatrix} 0 & \sqrt{5} & & & & \\ \sqrt{5} & 0 & \sqrt{8} & & & \\ & \sqrt{8} & 0 & 3 & & \\ & & 3 & 0 & \sqrt{8} & \\ & & & \sqrt{8} & 0 & \sqrt{5} \\ & & & & \sqrt{5} & 0 \end{pmatrix},\quad I_Y=\frac{1}{2i}\begin{pmatrix} 0 & -\sqrt{5} & & & & \\ \sqrt{5} & 0 & -\sqrt{8} & & & \\ & \sqrt{8} & 0 & -3 & & \\ & & 3 & 0 & -\sqrt{8} & \\ & & & \sqrt{8} & 0 & -\sqrt{5} \\ & & & & \sqrt{5} & 0 \end{pmatrix},\quad I_Z=\frac{1}{2}\begin{pmatrix} 5 & & & & & \\ & 3 & & & & \\ & & 1 & & & \\ & & & -1 & & \\ & & & & -3 & \\ & & & & & -5 \end{pmatrix} . \tag{A7}$$

This leads to the following relations:

$$\begin{aligned}
&\langle \pm m \mid I_X \mid \pm m' \rangle = 0 , \\
&\langle m \mid I_X \mid -m' \rangle = \langle -m \mid I_X \mid m' \rangle , \\
&\langle \pm m \mid I_Y \mid \pm m' \rangle = 0 , \\
&\langle m \mid I_Y \mid -m' \rangle = -\langle m \mid I_Y \mid m' \rangle , \\
&\langle \pm m \mid I_Z \mid \pm m' \rangle = \pm m \delta_{mm'} , \\
&\langle \pm m \mid I_Z \mid \mp m' \rangle = 0 ,
\end{aligned} \tag{A8}$$

where $(m = \frac{5}{2}, \frac{1}{2}, -\frac{3}{2})$. Equation (A8) enables us to calculate (A6) for the X, Y, and Z directions. For $\mathbf{H}_{\mathrm{rf}} || X$, the two conjugate transitions give the same sign,

$$(\mu_{12})_{\pm} = \gamma_x \hbar a_m b_{m'} \langle m \mid I_X \mid -m' \rangle \cos(\alpha_1 - \alpha_2) , \tag{A9}$$

whereas when $\mathbf{H}_{\mathrm{rf}} || Y$, they end up with the opposite sign,

$$(\mu_{12})_{\pm} = \pm \gamma_y \hbar a_m b_{m'} \langle m \mid I_Y \mid -m' \rangle \cos(\alpha_1 + \alpha_2) . \tag{A10}$$

Similarly when $\mathbf{H}_{\mathrm{rf}} || Z$, we get the opposite sign,

$$(\mu_{12})_{\pm} = \mp \gamma_z \hbar i a_m b_m m \delta_{mm'} \sin(\alpha_1 + \alpha_2) . \tag{A11}$$

In summary, two Zeeman conjugate components change sign only when $\mathbf{H}_{\mathrm{rf}} || Y$ or $\mathbf{H}_{\mathrm{rf}} || Z$. This effect is termed Zeeman interference.

[1] M. Mitsunaga, E. S. Kintzer, and R. G. Brewer, Phys. Rev. Lett. **52**, 1484 (1984).

[2] J. Mlynek, N. C. Wong, R. G. DeVoe, E. S. Kintzer, and R. G. Brewer, Phys. Rev. Lett. **50**, 993 (1983).

[3] N. C. Wong, E. S. Kintzer, J. Mlynek, R. G. DeVoe, and R. G. Brewer, Phys. Rev. B **28**, 4993 (1983).

[4] J. Mlynek, Chr. Tamm, E. Buhr, and N. C. Wong, Phys. Rev. Lett. **53**, 1814 (1984).

[5] E. S. Kintzer, M. Mitsunaga, and R. G. Brewer, following paper, Phys. Rev. B **31**, 6958 (1985).

[6] A. Wokaun, S. C. Rand, R. G. DeVoe, and R. G. Brewer, Phys. Rev. B **23**, 5733 (1981).

[7] M. A. Teplov, Zh. Eksp. Teor. Fiz. **53**, 1510 (1967) [Sov. Phys.—JETP **26**, 872 (1968)].

[8] T. P. Das and E. L. Hahn, *Nuclear Quadrupole Resonance Spectroscopy* (Academic, New York, 1958).

[9] In Ref. 1, the eigenvectors in (7) and (8) should be replaced by those without tildes. The eigenvectors of the left-hand side of (11) should be replaced by those with tildes. In (12b), m_i should be m_2.

[10] M. Tinkham, *Group Theory and Quantum Mechanics* (McGraw-Hill, New York, 1964), p. 101.

[11] L. E. Erickson, Phys. Rev. B **19**, 4412 (1979); **24**, 5388 (1981).

[12] R. M. Shelby and R. M. Macfarlane, Opt. Commun. **27**, 399 (1978).

[13] R. M. Shelby, R. M. Macfarlane, and R. L. Shoemaker, Phys. Rev. B **25**, 6578 (1982).

[14] B. R. Reddy and L. E. Erickson, Phys. Rev. B **27**, 5217 (1983).

[15] E. A. Whittaker and S. R. Hartmann, Phys. Rev. B **26**, 3617 (1982).

[16] R. M. Macfarlane and R. M. Shelby, Opt. Lett. **6**, 96 (1981).

[17] L. G. Rowan and E. L. Hahn, Phys. Rev. A **137**, 61 (1965); A. Schenzle, S. Grossman, and R. G. Brewer, *ibid.* **13**, 1891 (1976); Y. C. Chen, K. Chiang, and S. R. Hartmann, Phys. Rev. B **21**, 40 (1980); J. A. Kash and E. L. Hahn, Phys. Rev. Lett. **47**, 167 (1981); G. Bodenhausen, R. Freeman, G. A. Morris, and D. L. Turner, J. Magn. Reson. **28**, 17 (1977).